Toward Low-Cost, High-Efficiency, and Scalable Organic Solar Cells with Transparent Metal Electrode and Improved Domain Morphology

Myung-Gyu Kang, Hui Joon Park, Se Hyun Ahn, Ting Xu, and L. Jay Guo

(Invited Paper)

***Abstract*—We review our recent progress toward realizing future low-cost, high-efficiency, and scalable organic solar cells (OSCs). First, we show that the transparent electrodes based on metallic nanostructure is a strong candidate as a replacement of conventional indium tin oxide (ITO) electrode due to their superior properties, such as high optical transparency, good electrical conductivity, and mechanical flexibility, and the versatility that these properties can be adjusted independently by changing the linewidth and thickness of the metal grid structure. Furthermore, we exploited the unique optical properties due to the excitation of surface plasmon resonance by the metallic nanogratings to enhance the light absorption of organic semiconductors, and demonstrated enhanced power conversion efficiency than devices made using ITO electrode. In addition, we also investigated a new device fabrication process with a focus on the photoactive layer formation, which produces the most optimum bulk-heterojunction morphology compared with conventional annealing-based methods. Finally, we successfully demonstrated that these approaches are scalable to large-area and high-speed roll-to-roll processes. We believe that the works highlighted in this paper represent one step forward to realizing low-cost, high-efficiency, and large-area OSCs.**

***Index Terms*—Bulk heterojunction (BHJ), nanoimprint lithography (NIL), organic solar cell (OSC), roll-to-roll (R2R), surface plasmons (SPs), transparent and conductive electrode (TCE).**

Manuscript received November 24, 2009; revised January 14, 2010; accepted January 27, 2010. Date of publication April 29, 2010; date of current version December 3, 2010. This work was supported in part by the National Science Foundation, in part by the National Institute of Standards and Technology, in part by the King Abdulaziz City for Science and Technology, and in part by the Department of Energy. The work of M.-G. Kang was supported by a Rackham Predoctoral Fellowship. The work of H. J. Park was supported by a Rackham International Student Fellowship. The work of T. Xu was supported by a China Scholarship Council Scholarship. The first two authors (M.-G. Kang and H. J. Park) contributed equally to this study. Correspondence should be addressed to L. J. Guo.

M.-G. Kang was with the Solid State Electronics Laboratory, Department of Electrical Engineering and Computer Science, University of Michigan, Ann Arbor, MI 48109 USA. He is now with the National Institute of Standards and Technology, Gaithersburg, MD 20899-1000 USA (e-mail: myung-gyu.kang@nist.gov).

H. J. Park is with the Macromolecular Science and Engineering Center and Solid State Electronics Laboratory, Department of Electrical Engineering and Computer Science, University of Michigan, Ann Arbor, MI 48109 USA (e-mail: huijoon@umich.edu).

S. H. Ahn is with the Solid State Electronics Laboratory, Department of Electrical Engineering and Computer Science and Department of Mechanical Engineering, University of Michigan, Ann Arbor, MI 48109 USA (e-mail: happyash@umich.edu).

T. Xu and L. J. Guo are with the Solid State Electronics Laboratory, Department of Electrical Engineering and Computer Science, University of Michigan, Ann Arbor, MI 48109 USA (e-mail: xuting@umich.edu; guo@umich.edu).

Color versions of one or more of the figures in this paper are available online at http://ieeexplore.ieee.org.

Digital Object Identifier 10.1109/JSTQE.2010.2044634

I. Introduction

COST-EFFECTIVE and highly efficient renewable energy is becoming ever more important due to the rising energy price and the serious issue of global warming from the burning of fossil fuels. Solar energy is a nonexhaustible and green energy. Organic solar cells (OSCs) [1]–[3] offer a promising alternative to inorganic solar cells due to their low cost, easy fabrication, and compatibility with flexible substrates over a large area. Since their first report [4], the power conversion efficiency (PCE) of OSCs has steadily increased and now reached up to 4%–6% [5]–[10]. However, further enhancement of the PCE together with the low-cost fabrication is still required for practical applications [11]. This paper highlights the recent progress in the approaches we developed to produce low-cost, highly efficient OSCs, with a focus on future transparent conductive electrode (TCE) with enhanced functionalities and scalable and high-speed processing method of the organic materials.

Basic OSC structure consists of a number of organic semiconductor layers sandwiched between two electrodes. Most of the organic devices fabricated today use a thick, conductive metal layer as the rear electrode and a TCE as the front electrode, which receives light. TCE is very important component in any photosensitive optoelectronic devices, such as organic LEDs (OLEDs) and OSCs. An ideal TCE must be highly transparent to allow the maximum transmission of light, and it must also be conductive to provide uniform electrical current distribution. In addition to these properties, it must be mechanically and chemically stable, and should not cause the degradation of the active materials it contacts in the device structure. Among many candidates [12]–[25], indium-tin-oxide (ITO) is a highly doped degenerate semiconductor with optical bandgap above 3 eV; these features make it both conductive and transparent to wavelengths greater than approximately 400 nm [26]–[30]. As a result, ITO is the most common material for TCE and shows good performance in organic optoelectronic devices, such as OLEDs and OSCs. Though widely used [28], [29], [31]–[33], ITO faces several challenges for future low-cost, high-performance, large-area, and flexible applications [34]–[38]. The price of ITO drastically increases due to the limited supply of the indium and the increasing demand from the rapidly expanding liquid crystal display (LCD) display market. The migration of indium from ITO into organic layer can reduce the device performance [34], [39]. Moreover, it is not adequate for flexible applications because of the poor mechanical strength. Therefore, there is a strong need to find alternative materials to replace ITO as a high-transparency electrode.

1077-260X/$26.00 © 2010 IEEE

In addition to TCE, another important issue in OSC research is the morphology control of organic photoactive layers. Because the efficient dissociation of the photogenerated excitons and their charge transportation to each electrode through the effective pathways are determined by the nanostructures of electron-donor and acceptor in the photoactive layer, these morphologies directly affect the device performances, such as the PCE of solar cells. Accordingly, photoactive layer having bulk-heterojunction (BHJ) structures have been widely exploited for high-efficiency OSCs [5], [6], [40]–[42], because this type of structure permit us to access the interpenetrating nanoscale networks of electron-donor and acceptor with domain sizes on the order of exciton diffusion length, which has been measured to be 4–20 nm in organic semiconducting materials [43]–[47], and with large interfacial areas between the domains. Therefore, such network can facilitate efficient dissociation of photoinduced excitons at the domain interface. This advantage has made this approach a strong candidate for high-efficiency OSCs. However, randomly distributed blend morphologies in BHJ structures inevitably require annealing treatment to form effective pathway for the photogenerated charges to reach each electrode. Accordingly, optimizing blend morphology to provide effective charge pathway as well as large interfacial area is one of the most crucial issues to achieve high-efficiency OSCs using BHJ structures.

In this paper, we describe our recent efforts to solve the aforementioned issues in order to realize the future low-cost, high-efficiency, and scalable OSCs. First, we have developed a type of TCE based on metallic nanostructures. Developed transparent metal electrode (TME) [48] is in the form of a periodic nanoscale metal wire grid fabricated by nanoimprint lithography (NIL) [49] and has high optical transparency and good electrical conductivity. Moreover, unlike ITO, these properties are adjusted independently by changing the metal linewidth and thickness in the metal grid structure. In addition, we showed that such TME can be fabricated by a roll-to-roll (R2R) process for low-cost and scalable manufacturing (see Section II). Not only do metal electrodes provide excellent optical transmittance and electrical conductivity, but also the nanoscale metallic nanowire structures exhibit unique optical properties due to the excitation of surface plasmon (SP) resonance (SPR), which can be exploited in specially designed solar cells and demonstrated 35% PCE enhancement as compared to the devices made with conventional ITO electrode (see Section III). Finally, newly developed fabrication method [50] to achieve optimized morphology of photoactive layer, especially for polymer solar cells, toward high-efficiency solar cell and its application to scalable efforts will be also addressed (see Section IV). All devices shown in this paper were characterized under ambient condition without encapsulation.

II. TME for OSC Application

A. Introduction

TME [48] is in the form of nanoscale periodically perforated dense metal mesh films on glass or plastic substrate, as shown in Fig. 1. The high-transparency metal electrodes are fabricated by NIL [49] and have several advantages over other highly transparent electrodes including ITO. First, the work function of nanopatterned TME can be easily tuned by choosing different metal materials, which allows systematic studies of the effect of the electrode work function on the device performance. Second, a high electrical conductivity can be achieved without seriously compromising the transparency [48]. Third, the light absorption and the resulting PCE of OSC can possibly be increased by means of a light trapping phenomenon induced by the grating structure [51]–[54]. Lastly, large-area OSC having a TME could be realized at a low cost by using a newly developed R2R nanoimprint technique [55].

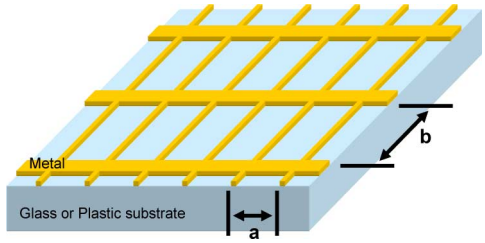

Fig. 1. Schematic of TMEs. a: Main grating for TME. b: Secondary grating for electrical connectivity of main grating a.

B. Design of TMEs

The TMEs are fabricated based on two design considerations: 1) the linewidth of the metal mesh is designed to be subwavelength to provide sufficient transparency and to minimize light scattering and reflection and 2) the period of the mesh "a" in Fig. 1 is chosen to be submicrometer to ensure the uniformity of the current collection from the organic semiconductors. This mesh serves as the main part of the TME. An orthogonal mesh with a period of "b" is used to ensure the electrical connectivity of the main grating lines in case some of lines may be disconnected due to defects in the fabrication processes. The optimum period of metal grating can be determined by considering the sheet resistance of poly(3,4-ethylenedioxythiophene): poly(styrenesulfonate) (PEDOT:PSS), which in turn determines the voltage drop between the adjacent metal lines, as the photocurrents are collected. The total voltage drop in the device area, assumed to be 0.1 cm^2, can then be estimated by considering the number of metal lines in the whole device area at certain period of grating. If we allow the total voltage drop to be about 10 mV, then the optimum period can be determined [25]. As shown in Fig. 2, the optimum period of the TME can be found in the red area. The more the red in the area, the better the OSC performance will be. Outside the red area, the TME will still be able to collect generated photocurrent, but with reduced efficiency.

C. Fabrication of TME on Glass Substrate

Such large-area TMEs are fabricated by NIL [49], [56], which is ideal for this application due to its inherent high resolution and high throughput features. The details of the fabrication of the mold for NIL and TME are described in previous publications [25], [48]. Fig. 3(a) shows the fabricated mold with a period of 700 nm and linewidth of 70 nm for the main grating. The secondary grating with a period of 10 μm and a linewidth of 400 nm was used to ensure the electrical connectivity of the main grating while minimizing the transmittance loss. NIL created large-area TME successfully, as shown in Fig. 3(b).

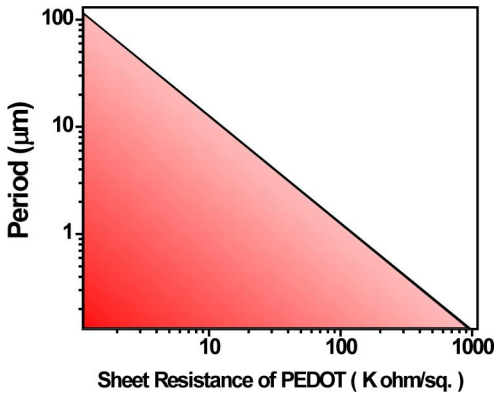

Fig. 2. Calculated optimum period of the nanopatterned metal grating in TME as a function of the sheet resistance of the PEDOT:PSS layer. Choosing the metal grating period and the PEDOT sheet resistance within the red region will lead to negligible loss of photocurrent. Copyright Wiley-VCH Verlag GmbH & Co. KGaA. Reproduced with permission from [25].

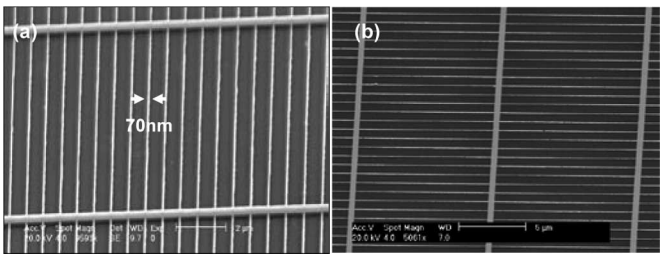

Fig. 3. SEM images of (a) mold with a period of 700 nm and linewidth of 70 nm and (b) fabricated TME using the mold of (a) on glass substrate. Copyright Wiley-VCH Verlag GmbH & Co. KGaA. Reproduced with permission from [25].

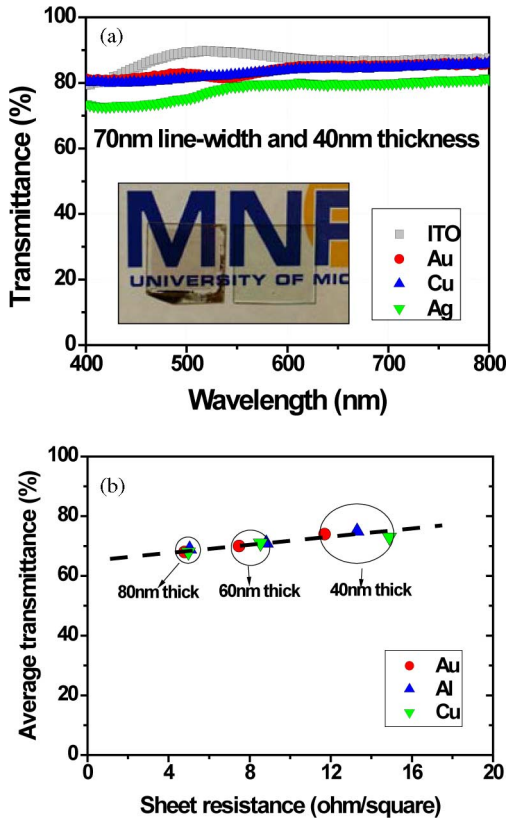

Fig. 4. (a) Optical transmittance of the ITO and TMEs with a period of 700 nm and linewidth of 70 nm. (b) Average transmittance versus sheet resistance of TMEs with a linewidth of 120 nm. Copyright Wiley-VCH Verlag GmbH & Co. KGaA. Reproduced with permission from [48].

Nanoscale patterning of the metal film provided high-transparency conductive electrode, whose transmittance is comparable to the commercially available standard ITO electrode, as shown in Fig. 4(a).

High-transparency metal electrodes using Au, Cu, and Ag are shown, but any other metals can be used for this purpose as well. Fig. 4(b) shows the typical behavior of the average transmittance of the metal electrode in the visible range as a function of different sheet resistance. TMEs with a linewidth of 120 nm were considered in this case. As shown in Fig. 4(b), the sheet resistance of the metal electrode can be decreased to less than a few ohms per square with only a small decrease of the average transmittance. This characteristic is another advantage over an ITO electrode, in which the sheet resistance has to be compromised in order to achieve high transmittance. Low sheet resistance (i.e., high electrical conductivity) of the transparent electrode is one of the most important aspects in OSCs, especially in large-area devices because the resistance of the transparent electrode in large-area OSC causes additional reduction of the device fill factor (FF), resulting in reduced PCE. Therefore, developed TMEs are very promising, not only because they can avoid the disadvantage of the ITO electrode, but also because they can meet the requirement of both high optical transmittance and high electrical conductivity, for large-area OSC applications.

D. Fabrication of TME on Plastic Substrate

The TMEs we developed [48] showed promising potential as a replacement for the ITO electrode. However, the lithographic technique used, i.e., NIL, for the fabrication of TME is not compatible with the flexible substrate. The conventional NIL requires high pressure and high temperature when imprinting thermoplastic material, which can cause deformation of the flexible substrate. Therefore, other nanoscale patterning techniques that can easily produce the nanostructure metal mesh pattern are needed. We have developed a nanolithography based on metal transfer printing using a flexible poly(dimethysiloxane) (PDMS) stamp, as shown in Fig. 5, which can produce nanoscale metal patterns directly on plastic substrate [57] [e.g., polyethylene terephthalate (PET)] or polymer (e.g., PEDOT:PSS) coated PET substrate [58].

Fig. 6 shows the optical transmittance spectra, photograph, and SEM image of the high-transparency Cu mesh electrode fabricated by metal transfer printing on PEDOT:PSS-coated PET substrate. Though other metals such as Au and Ag can be used than Cu, here we show the result of Cu mesh electrode because of its much lower cost. Cu, being one of the cheapest metals, is well suited for practical low-cost and large-area OSC applications.

The fabricated Cu electrode was found to be much more flexible than the ITO by simple bending test and the results are shown in Fig. 7. In the case of the transparent Cu electrode, it can

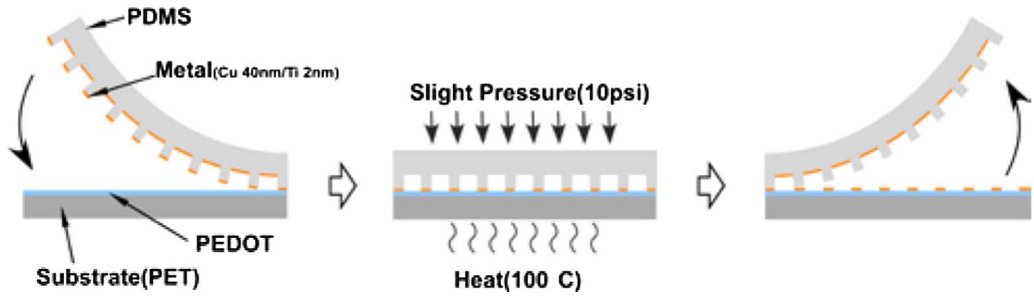

Fig. 5. Schematic of the fabrication of nanopatterned metal electrode on a PEDOT:PSS coated plastic substrate by using a flexible PDMS stamp. Copyright Wiley-VCH Verlag GmbH & Co. KGaA. Reproduced with permission from [25].

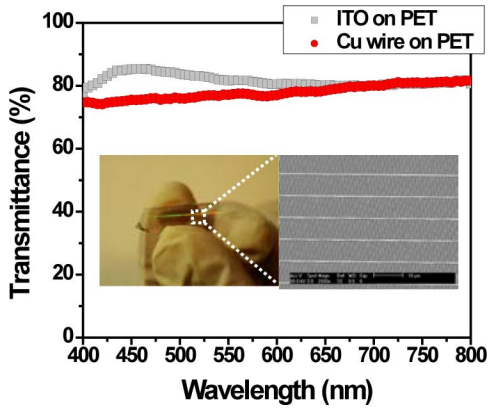

Fig. 6. Optical transmittance spectra of ITO electrode and Cu mesh electrode on PET substrate. (Inset) Photograph and SEM image of the high-transparency Cu mesh electrode.

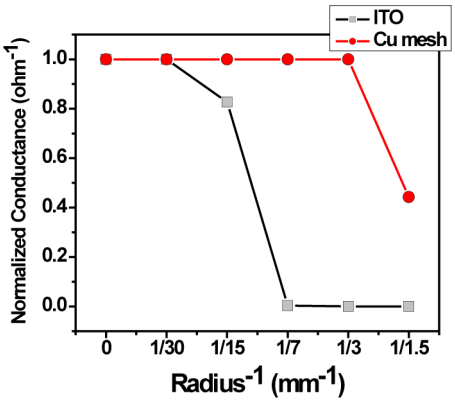

Fig. 7. Normalized conductance versus inverse of the radius of curvature of the Cu mesh and the ITO electrode.

be bent to about 3 mm radius of curvature with no degradation of the conductance. On the other hand, the ITO exhibited a reduction of the conductance even at a radius of ~30 mm, which can reach close to zero due to the microcracking in ITO film on the order of 20 μm after the bending.

The fabrication of the nanopatterned metal electrode using the metal transfer printing technique can be extended to cost-effective and large-area fabrication, such as roll-to-roll NIL (R2RNIL) [55], [59] with the use of flexible molds. As a proof of principle, we fabricated nanoscale metal (e.g., Au) gratings on large-area PET substrates using an R2R process [58] (see

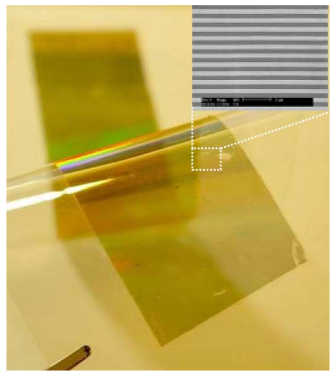

Fig. 8. Photograph of large area (32 mm × 184 mm) Au nanogratings fabricated by R2R process. (Inset) SEM image of fabricated Au nanogratings.

Fig. 8). The inset in Fig. 8 shows the SEM image of transferred Au nanograting on PET substrate. Other metals such as Ag and Cu can also be easily fabricated using such a continuous process.

E. OSCs Using TME

To evaluate the potential use of the nanopatterned metal electrode as a high-transparency conducting electrode for OSCs, BHJ devices based on a blend of poly(3-hexylthiophene) (P3HT) and [6,6]-phenyl C_{61} butyric acid methyl ester (PCBM) as active material were fabricated using such an electrode and compared to the one made with the commercial ITO electrode on glass substrate. The fabricated solar cells have an area of approximately 0.1 cm^2 (circular shape shadow mask with 3.5 mm diameter). The patterned Al cathode has isolated island-type geometry to exclude the overestimation of the photocurrent when a crossbar-type geometry is used [25], [60]. The issue of the photocurrent overestimation in case of crossbar-type device fabrication will be discussed in Section IV. The measured current density (J) versus voltage (V) characteristics at 1 sun air mass (AM) (AM 1.5G) are shown in Fig. 9. The results reported in Fig. 9 are averaged using the data obtained by at least 20 cells for each electrode. The J–V characteristics of the solar cells having the nanopatterned TMEs and ITO electrode are very similar to each other, thus indicating that such electrodes are interchangeable. All devices showed a PCE of ~2%. Note that such PCE is lower than the ones reported in literature because all of our devices were fabricated and tested in ambient environment with no special control of oxygen and moisture. PEDOT:PSS and

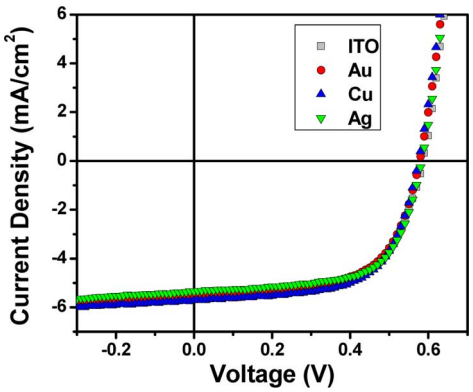

Fig. 9. Current density versus voltage characteristics of similarly fabricated OSCs with varied electrodes, including nanopatterned Au, Cu, Ag, and ITO electrode. Copyright Wiley-VCH Verlag GmbH & Co. KGaA. Reproduced with permission from [25].

the blend material were spin-coated and baked in a N_2 glove box. The device fabricated with the metal electrode on flexible PET substrate also performed similarly to the conventional ITO device. These results indicate that the TME can potentially replace the ITO electrode with better flexibility and lower cost.

III. SP-Enhanced Efficiency of OSCs Using Transparent Silver Nanowire Electrode

A. Introduction

To enhance the PCE of the device, both the light absorption in the organic layer and the electrical transport of the photogenerated carriers must be enhanced [2], [3], [61]. High absorption of the incident light can be achieved by using a thick organic active layer. However, a thick active layer increases the series resistance and recombination loss due to the low carrier mobility of the organic materials, resulting in a reduced FF, and thus, reduced efficiency [62]. Therefore, an effective approach to enhance the efficiency of a thin-film OSC is to increase the light absorption of the organic film without having to increase the photoactive layer thickness. For this purpose, several light trapping approaches including a folded configuration [63], diffraction grating [51], [53], [64], photonic crystal [65], and SPR [66]–[73] have been investigated and have demonstrated promising results. Among these approaches, the utilization of the SPR in metallic nanostructures is one of the most promising ways as SPs exhibit strongly enhanced electromagnetic fields in the vicinity of metal by the incident light, which can lead to increased optical absorption in the organic film, and therefore, higher efficiency. Ag nanoparticles have been widely used to increase optical absorption by the SPR effect [67], [70], [71]. However, the field enhancement from metallic nanoclusters is highly localized around the nanoclusters and the possible exciton quenching can limit the utility of such nanoclusters in thin-film OSCs [67]. Moreover, most of the works using Ag nanoparticles have been done on conventional device structure in which ITO is used as a transparent electrode. It would be very attractive if the transparent electrode itself can excite the SPR, and thus, increasing the optical absorption of the organic layer of the device. Such attempts have been reported using randomly perforated Ag films and periodic Ag gratings [72], [73]. Even though these approaches demonstrated relative enhancement of the optical absorption by the SPR in OSCs, none of them could compare with standard ITO devices, due to the overall much lower efficiency obtained by these devices. Recently, we have demonstrated the enhancement of PCE of the organic thin-film solar cell using periodic Ag nanowire electrodes, as compared to that of conventional device using ITO electrode through the SPR in Ag nanowire electrodes [74].

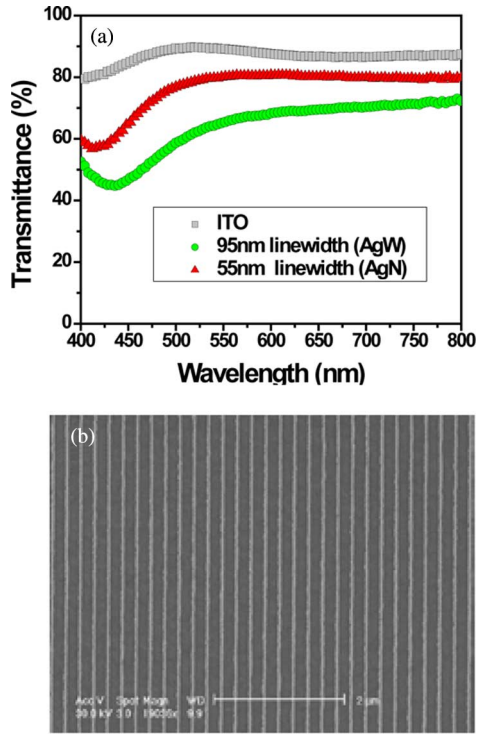

Fig. 10. (a) Optical transmittance of the ITO, AgW, and AgN electrode. (b) SEM image of the AgN electrode.

B. Fabrication of Ag Nanowire Electrodes

The period and thickness of Ag nanowire electrodes investigated in this paper are 220 and 40 nm, respectively. Two sets of Ag nanowire electrodes with different linewidth (95 and 55 nm) are prepared based on our initial simulation results that showed different field-enhancement factors for the Ag nanogratings with different duty cycles. Ag nanowires with wide (95 nm) and narrow linewidth (55 nm) are referred to as AgW and AgN, respectively, hereafter. These Ag nanowire electrodes are fabricated using NIL and shadow evaporation technique [48]. Fig. 10 shows the optical transmittance of the fabricated Ag nanowire electrode together with that of conventional ITO electrode and an SEM image of AgN nanowire electrode.

As shown in Fig. 10(b), uniform, transparent Ag nanowire electrodes are successfully fabricated by NIL. The average transmittance, referenced to air in the visible range, of Ag nanowires with a linewidth of 95 and 55 nm, and ITO electrode is 58%, 77%, and 87%, respectively. Periodically, patterned Ag films exhibited the light absorption at specific wavelength range by SPR, as shown in optical transmittance spectra. The resonance

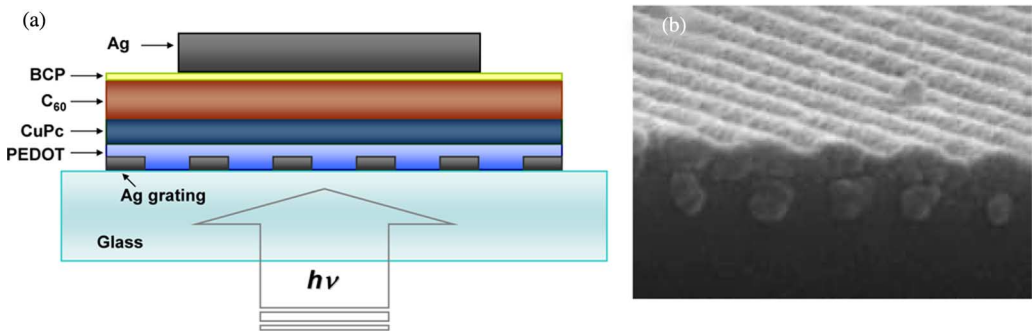

Fig. 11. (a) Schematic and (b) SEM image (without Ag cathode) of the fabricated device.

wavelength is around 425 nm and is expected to red shift to the absorption band of the organic semiconductor when it is coated over the Ag nanowires due to increased refractive index [75].

C. OSCs Using Transparent Ag Nanowire Electrodes

Small molecular weight OSC (SMOSC) using copper phthalocyanine (CuPc) and buckminsterfullerene (C_{60}) as an electron donor and acceptor, respectively, were fabricated. The fabricated devices have the layered structure of anode (Ag nanowire or ITO), PEDOT:PSS, CuPc, C_{60}, bathocuproine (BCP), and cathode (thick Ag film) from bottom to top. The cathode was formed by depositing Ag through the circular-shape shadow mask with the diameter of 1 mm. Fig. 11 shows (a) a schematic of the fabricated device and (b) cross-sectional SEM image of a device fabricated using the Ag nanowires, but without the thick Ag cathode.

As shown in Fig. 11, there is a difference in cross-sectional view between the schematic and the real sample due to the thickness (40 nm) of Ag nanowire electrodes and nature of thermal evaporation of small molecules. Fabricated samples have a sinusoidal shape with a maximum height difference of about 30 nm. The effects of nonplanar shape of the device are discussed later. Conductive PEDOT:PSS was used for the following three purposes: 1) it facilitates the transport of the photogenerated holes to the Ag nanowire electrodes; 2) it prevents the direct contact of organic active layer to Ag nanowire, which reduced the chance of the device shunt; and 3) it would also block the potential exciton quenching by the metal. Several devices with different thicknesses of the organic layers were fabricated to investigate the dependence of the optical field enhancement by the SPR on the organic layer thicknesses in a given Ag nanowire geometry. For all cases, the thickness of the PEDOT:PSS and BCP was fixed at 30 and 8 nm, respectively. The total organic layer thickness was controlled by changing the thickness of CuPc and C_{60} while attempting to keep the ratio of two materials the same. Table I summarizes the thicknesses of the organic layers of the fabricated devices. For all considered cases, devices were fabricated using commercial ITO, or AgW and AgN electrodes. More than 20 devices for each case were fabricated and measured.

The measurement results showed that the device parameters such as V_{oc} and FF were similar for both the ITO and Ag devices at each organic layer thickness (see Table I) except device #5, which showed much reduced V_{oc}, ~0.37 V that can be attributed to the shunt path between the edge of the Ag nanowires and the top cathode due to the very thin organic layer (70 nm). Devices #1 and #2 having relatively thicker organic layer showed smaller FF (0.4) for both ITO and Ag devices as compared with that (0.5) for the devices #3 and #4 with thinner layers. This is because thicker organic layer presents higher resistance to the photocurrent due to low carrier mobilities of organic materials. Similar V_{oc} and FF for both ITO and Ag devices indicate that the patterned Ag electrode did not affect the device fabrication using thermal evaporation of small molecule materials and the collection of the photogenerated carriers. While having similar V_{oc} and FF for all devices, the short-circuit current (J_{sc}) showed a dramatic difference. Overall, the J_{sc} of the ITO device decreases with reducing organic layer thickness because of the lower absorption in thinner devices. In sharp contrast, the AgN device showed enhanced J_{sc} as the organic layer thickness decreases, as shown in Fig. 12(a). For thick organic layers (devices #1 and #2), the J_{sc} of the device made with AgN is comparable to that of the ITO device. For organic layers thinner than 100 nm (devices #3, #4, and #5), the J_{sc} of the device with AgN was enhanced as much as 43% compared to that of ITO device, as the thickness of the total organic layer decreases to 70 nm. This is consistent with our simulation results that showed stronger SP enhancement effect for thinner organic layers. The device made with AgW also showed a similar behavior to AgN device, but the overall enhancement was lower due to the low transmittance of the AgW electrode, as shown in Fig. 10(a). Fig. 12(a) shows the dependency of the J_{sc} and PCE of each device (ITO, AgN, AgW device) on the thickness of the organic layer. Fig. 12(b) shows the *J–V* curve of the device #4 that exhibits the highest enhancement of the J_{sc} and the overall PCE. In fact, the device #5 showed the highest enhancement of the J_{sc}, but the PCE was low due to the low V_{oc}.

Each device has a different thickness of the organic layer resulting in different absorption efficiency. Thus, the enhancement factor of the J_{sc} of the Ag devices was extracted by normalizing

TABLE I
THICKNESS OF THE ORGANIC LAYERS OF THE FABRICATED DEVICES

Device #	Thickness (nm)				
	PEDOT	CuPc	C_{60}	BCP	Total
1	30	28	44	8	110
2	30	25	35	8	100
3	30	20	32	8	90
4	30	16	26	8	80
5	30	12	20	8	70

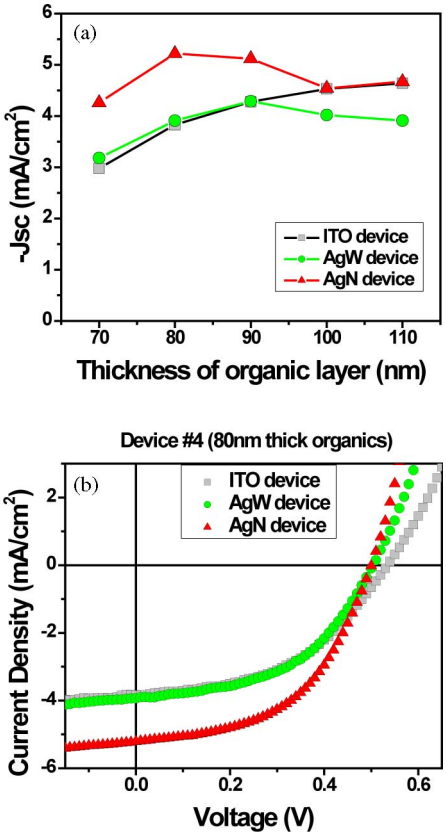

Fig. 12. (a) J_{sc} versus thickness of the organic layer of the devices fabricated. (b) J–V curves of the device #4 in which AgN device exhibited highest enhancement of the J_{sc} and overall PCE.

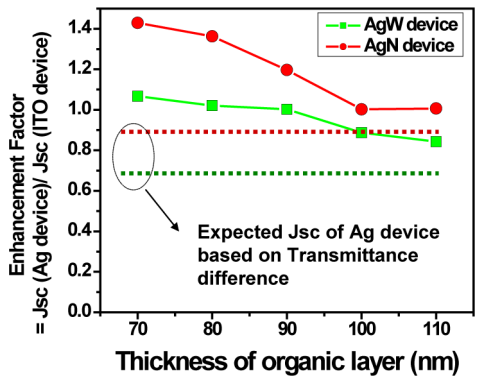

Fig. 13. Enhancement factor versus thickness of the organic layers. Dotted lines show the expected J_{sc} of the Ag device based on the transmittance of each electrode without absorption enhancement.

the J_{sc} of the Ag devices with that of the ITO device and is shown in Fig. 13. The dotted lines show the expected J_{sc} purely based on the transmittance of each electrode when there is no absorption enhancement. We believe that the SPR enhances the light field and this lead to the enhanced absorption efficiency accordingly, thus resulting in the increased J_{sc}. The difference between actual enhancement (solid line) and expected enhancement (dotted line) can be regarded as a net enhancement factor when the transmittance of each electrode is considered. The actual enhancement in the AgW device is much lower than that of

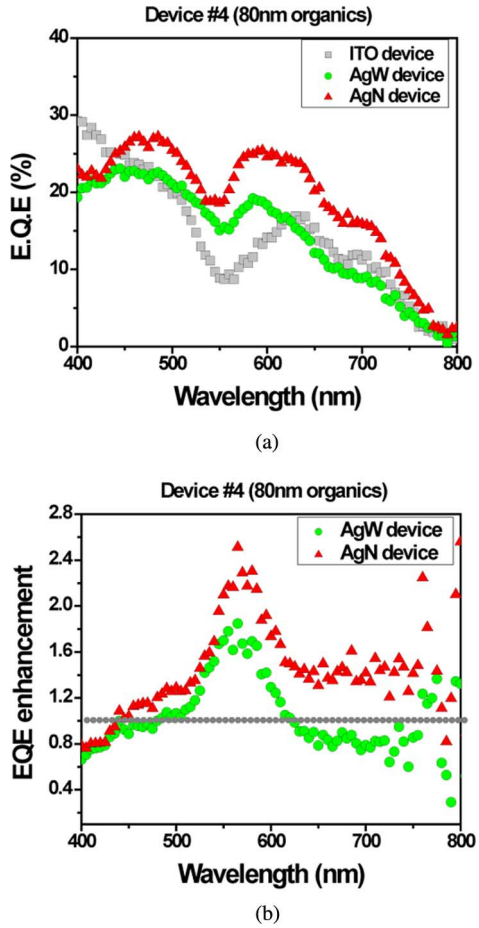

Fig. 14. (a) Measured EQE spectra of the ITO, AgW, and AgN device in case of 80-nm-thick organic layers (device #4). (b) EQE enhancement factor of the AgW and AgN device as referenced to the ITO device. Note the scattered data points around 800 nm was due to the low EQE in ITO control device, which was magnified by the numerical divisions.

the AgN device. This result tells us that the transmittance of the anode is also a very important factor for the device to achieve high PCE. As a result of the increased J_{sc}, absolute PCE enhancement was achieved for the device with AgN electrode due to the increased J_{sc}, as compared to the device with ITO electrode. For device #3 with organic layer thickness of 90 nm, the PCE of the ITO and AgN device is 1.2% and 1.41%, respectively, which leads to about 18% enhancement of the PCE. For device #4 with organic layer thickness of 80 nm, the enhancement achieved was even higher. About 35% PCE enhancement was achieved with the PCE of 0.96% and 1.32% for the ITO and AgN device, respectively.

In order to get the conclusive evidence that increased J_{sc} is due to the enhanced absorption due to the excitation of SP, incident photon-to-current efficiency (IPCE) was measured for each device. The obtained external quantum efficiency (EQE) spectra for device #4 are shown in Fig. 14(a). The AgN device showed EQE enhancement for wide visible range. Since the EQE is approximately proportional to the absorption efficiency, the increase in J_{sc} can be attributed to the enhanced absorption by the organic semiconductors in the Ag nanowire electrode.

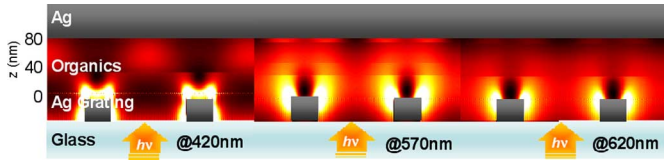

Fig. 15. Optical field intensity inside AgN device having the total organic layer thickness of 80 nm at a wavelength of 420, 570, and 620 nm, from left to right.

The enhancement factor of the absorption efficiency of the Ag device relative to the ITO device as a function of wavelength can be extracted from the ratio of the EQE between the Ag devices and the ITO device. As shown in Fig. 14(b), AgN device showed more EQE enhancement than ITO device over a wavelength range 450–700 nm. About a 2.5-fold EQE enhancement was achieved at around 570 nm for the AgN device #4.

Simulations based on rigorous coupled-wave analysis (RCWA) were performed to map the internal optical field of the device structure shown in Fig. 11(a). Measured complex refractive-index data for each organic layer were used. Fig. 15 shows the optical field profile inside the structure at different wavelengths in case of AgN device #4 having total thickness of organic layer of 80 nm. From the Fig. 14(b), at a wavelength of around 420 nm, the AgN device shows an EQE enhancement factor lower than 1 (ITO shows better EQE). The EQE of the AgN device showed the strongest enhancement at a wavelength of around 570 nm and moderate enhancement at a wavelength of around 620 nm. Simulation results match well with these experimental ones, as shown in Fig. 15. One thing to note in Fig. 15 is that the highest optical field is at the vicinity of the grating structure, where the PEDOT:PSS layer is. Therefore, by reducing the PEDOT:PSS thickness while maintaining the same total thickness of the organic layers, will increase the absorption efficiency of the organic active material, resulting in more enhanced photocurrent, and thus, enhanced device efficiency. More simulation works for optimal device structure and dimension that can further enhance the PCE of the device are currently under way.

Are there other effects which can explain the observed enhancement of J_{sc}? There are two other possibilities: light trapping by the light diffraction in grating structure and the device area increase caused by using 40-nm thick Ag grating as an anode. Both can be shown to play little role in our device because the 220-nm period grating has no diffraction effect in the visible absorption band of the organic semiconductors; and devices fabricated with thicker metallic wires showed very similar device performance including PCE.

IV. Morphology-Optimized Scalable BHJ Polymer Solar Cells

A. Introduction

It has been well known that BHJ morphologies of photoactive layer in polymer solar cells, composed of electron-donor and acceptor, strongly depend on their processing conditions. A number of studies have been dedicated to finding the efficient ways to optimize BHJ blend morphology using P3HT: PCBM as a model system. Thermal annealing (TA) and solvent-assisted annealing (SAA) treatments after spin-casting the blend film are widely accepted as general approaches to obtain well-organized interpenetrating networks composed of highly crystallized components can be achieved [5], [6], [42]. However, recent works that investigated phase separation of components in the direction normal to the film and electrode surface revealed that the BHJ structures fabricated by these methods do not produce optimized morphology: a nonuniform vertical distribution exists with P3HT phase dominant near the cathode and PCBM phase dominant near the anode [76]–[79]. Such nonuniform distribution is opposite to the ideal solar cell structure that requires a donor-rich phase near the anode and an acceptor-rich phase near the cathode, and therefore, unfavorable to charge transport to the electrodes. In addition, both annealing processes require relatively long processing time (e.g., tens of minutes for TA [6] or a few hours for SAA [5]) and spin-casting deposition can only be applied to small and rigid substrate, making these approaches not suitable to practical large area and mass production of polymer solar cells. Even though high-speed fabrication processes on flexible substrates have been reported, their device performances still cannot compare to those polymer solar cells made by spin-casting followed by annealing treatments [80]–[82]. This is because the traditional high-speed R2R coating method may not provide sufficient annealing time for crystallization, and hence, result in lower device efficiency [80]–[82]. Recently, we introduced a novel route that allows Evaporation of Solvent through Surface ENCapsulation and with Induced ALignment (ESSENCIAL) of polymer chains by applied pressure (see Fig. 16) [50]. The essence of this approach is to utilize a gas-permeable silicone cover layer for solvent evaporation that simultaneously protect the otherwise free polymer surface and induce shear flow of the blend solution by an applied pressure. This process not only leads to optimized morphology having more uniform distribution and high crystallinity of the components favorable for charge generation and transportation that cannot be achieved by conventional TA and SAA methods, but also is applicable to high-speed dynamic process that is ultimately demonstrated in an R2R process while preserving high device performances. Polymer solar cells fabricated in this paper have the following planar configuration: transparent substrate/ITO/PEDOT:PSS (∼45 nm)/P3HT:PCBM (∼240 nm)/LiF (∼1 nm)/Al (∼80 nm, island-type circular shape with 3.5 mm diameter).

B. BHJ Morphologies Depending on Processing Methods

The effects of different processing methods on the crystallinity of the conjugate polymer were investigated first. The chain ordering of the conjugate polymer in a BHJ structure is one of the essentials to achieve improved crystallinity for high-efficiency solar cell, because the improved organization of polymer chains facilitates hole transport and the long conjugation length enhances the absorption of light resulting in efficient exciton generation [3]. The absorption spectrum of the blend film fabricated by ESSENCIAL method was compared with that made by the spin-casting method in Fig. 17. To further evaluate the efficiency of the ESSENCIAL method, the samples treated by TA and SAA after spin-casting, which were generally used to improve the crystallinity of the P3HT, were also

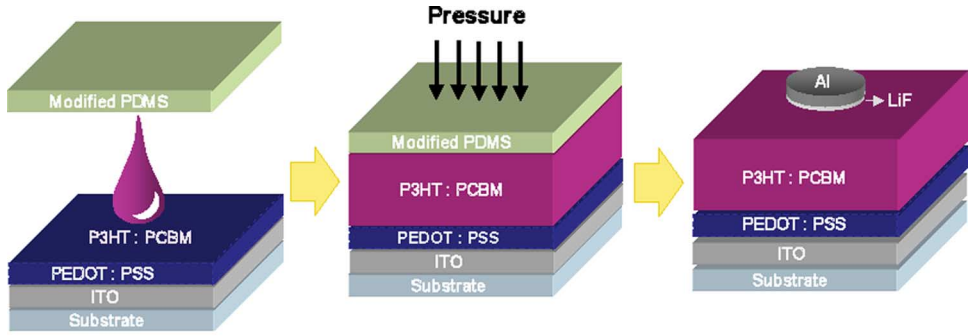

Fig. 16. Schematic of the ESSENCIAL process for fabricating polymer solar cells. (a) Applying blend solution. (b) Active layer formation during solvent evaporation through a gas-permeable silicone cover layer under pressure. (c) Isolated island-type cathode deposition on top of polymer blend film after removing the PDMS stamp. Copyright Wiley-VCH Verlag GmbH & Co. KGaA. Reproduced with permission from [50].

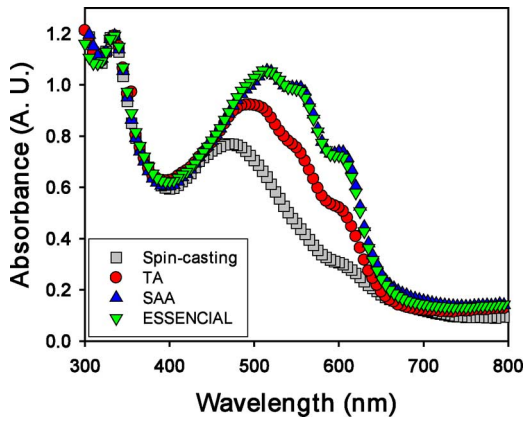

Fig. 17. Absorption spectra of the blend films. The spectra have been normalized to the PCBM peak around 325 nm. Copyright Wiley-VCH Verlag GmbH & Co. KGaA. Reproduced with permission from [50].

examined. The enhanced vibronic peaks in the absorbance spectra as well as significant red shift, which indicate a higher degree of ordering of P3HT chains [83], were observed in the ESSENCIAL sample. Additionally, this processing could be completed in just a few seconds, but the enhancement found in this sample was much higher than that in samples thermally annealed for 20 min and was even comparable to that of the solvent-annealed sample in which P3HT crystals were slowly grown for 2 h. Such property permits this method to be applied to high-speed R2R process and can produce well-ordered P3HT domains.

In addition to improved polymer crystallinity, the nanodomains of each blend component should be well connected in order for the holes from charge-separated excitons to be effectively transported to anode, and the electrons to cathode through continuous pathways. However, the nonuniform distribution of the donor and acceptor components found in spin-casted sample, even after TA or SAA, is not helpful to the effective charge transport to the electrodes [76]–[79]. This nonuniform distribution of components in vertical direction is a consequence of the surface energy difference between P3HT (26.9 $\mathrm{mN{\cdot}m^{-2}}$) and PCBM (37.8 $\mathrm{mN{\cdot}m^{-2}}$), which pushes P3HT to the low surface energy air surface to minimize the overall free energy [77]–[79]. In contrast, much uniform vertical distribution is expected for

TABLE II
WEIGHT RATIO OF PCBM TO P3HT CALCULATED FROM XPS FOR DIFFERENCT PROCESSING METHIDS

Method	Weight ratio (PCBM:P3HT)
TA	0.411 ± 0.058
SAA	0.483 ± 0.055
ESSENCIAL	0.855 ± 0.040

films prepared by the ESSENCIAL process, because the gas-permeable silicone film effectively provides a higher surface energy than that of air surface. X-ray photoelectron spectroscopy (XPS) results presented in Table II clearly illustrate these trends. Though the weight ratio of PCBM to P3HT in the blend solution is 1 : 1, the weight ratio of PCBM to P3HT of thermal- and solvent-assisted annealed samples measured at the top surface were reduced to 0.411 and 0.488, respectively, which indicates a large accumulation of P3HT at the top. But the ESSENCIAL sample produced much more balanced value (0.855), which implies more uniform distribution of components in the vertical direction.

In order to confirm that the uniformly distributed components in ESSENCIAL-treated sample are truly beneficial to effective charge transport by providing more continuous pathways through the film, we constructed hole- and electron-only devices in order to evaluate the charge transport properties in the phase-separated blend film [84], [85]. The hole-only device was fabricated by replacing LiF with high work-function molybdenum oxide ($\mathrm{MoO_3}$) to block the injection of electrons from the Al cathode, and electron-only device by using low work-function cesium carbonate ($\mathrm{Cs_2CO_3}$) to replace PEDOT:PSS to block the hole injection from the ITO anode [85]. The log$J$–log$V$ plots of hole- and electron-only devices, fabricated by different methods, are measured under dark condition, and both hole- and electron mobility were calculated by fitting data to the space-charge-limited-current (SCLC) model at low voltage [86]

$$J = \frac{9}{8}\varepsilon_0\varepsilon_r\mu\frac{V^2}{L^3}$$

where $\varepsilon_o\varepsilon_r$ is the permittivity of the component, μ the carrier mobility, and L the thickness of the organic layer.

TABLE III
CALCULATED CARRIER MOBILITIES DEPENDING ON THE DIFFERENT PROCESSING METHODS

Method	Carrier mobility (10^{-4} $cm^2V^{-1}s^{-1}$)		Ratio (μ_e/μ_h)
	Electron (μ_e)	Hole (μ_h)	
TA	-	1.57	-
SAA	4.95	3.29	1.50
[a]ESSENCIAL	14.61	12.55	1.16

[a]ESSENCIAL sample was further treated by heat for 1 min.

Table III shows the calculated hole and electron mobilities, depending on the processing methods. The most optimized transport pathways for both charge carriers were achieved in the post-heat-treated ESSENCIAL sample, and well-balanced mobilities ($\mu_e/\mu_h \sim 1.2$) were obtained. Even though the electron mobility of the thermally annealed device was not well matched with the SCLC model, the significantly lower expected values ($10^{-8} \sim 10^{-7}$ $cm^2 \cdot V^{-1} \cdot s^{-1}$) do not affect any conclusions here.

As a last aspect, the domain size in the BHJ structures and their effects on the exciton quenching were investigated using atomic force microscopy (AFM) and photoluminescence (PL) (see Fig. 18). Compared with the nonuniform mixture where one phase is dominant at one surface, more uniformly mixed donor and acceptor phases throughout the film are expected to have finer interpenetrating nanodomains that are advantageous to efficient dissociation of photogenerated excitons, and hence, result in suppressed PL from the donor polymer. It has been reported that the PL of annealed sample is enhanced as compared with just spin-casted film, because the higher crystallinity induced by annealing gives relatively poor exciton dissociation due to the reduction of interfacial contact area between the donor and acceptor domains [87]. On the other hand, the improved charge transport of the annealed samples due to increased crystallinity can offset the poor exciton dissociation effect, still producing high-efficiency solar cells [61]. Therefore, the solvent-assisted annealed sample having higher crystallinity than the thermal-annealed sample showed well-defined domains in AFM phase images, and this improved crystallinity induced the enhancement of PL in Fig. 18(d). As for the heat-treated ESSENCIAL sample, finer interpenetrating networks than the solvent-assisted annealed sample were expected due to the more uniform distribution of the blend, and well-defined nanodomains were much more discernable in AFM phase images. These uniformly distributed and fine-interpenetrating nanodomains not only permit good charge pathways, but also facilitate the efficient exciton dissociation; therefore, suppressing the PL from the donor, and consequently, gave the lowest PL [see Fig. 18(d)].

Another remarkable merit of the ESSENCIAL-based device is that PEDOT:PSS layer used on top of transparent anode in OSCs was not indispensable to this processing. PEDOT:PSS is the most widely used buffer layer between ITO anode and the active organic semiconductor to improve the performance of the polymer solar cells. One of the important roles of this PEDOT:PSS layer is to provide efficient electron blocking [88] to prevent electron leakage from the BHJ acceptors [89]. If PEDOT:PSS is not used, our experiments on the annealed devices after spin-casting showed significant drop of FF (e.g., from 0.65 to 0.55) that result in much reduction in PCE (see Fig. 19). However, the ESSENCIAL-based device shows only small drop of FF (e.g., from 0.69 to 0.67) that result in negligible effect to PCE, as shown in Fig. 19. This effect is consistent to the improved morphology in ESSENCIAL devices discussed earlier. Because in the devices with spin-casted film, large amount of PCBM are nonuniformly assembled near the ITO anode, inducing electron leakage. However, the uniform distribution of components in ESSENCIAL-based devices drastically reduces these electron leakage pathways. Therefore, this observation alone can be an important evidence for the uniform distribution of components in the blend film fabricated by the ESSENCIAL method. Moreover, avoiding the use of PEDOT:PSS can significantly reduce

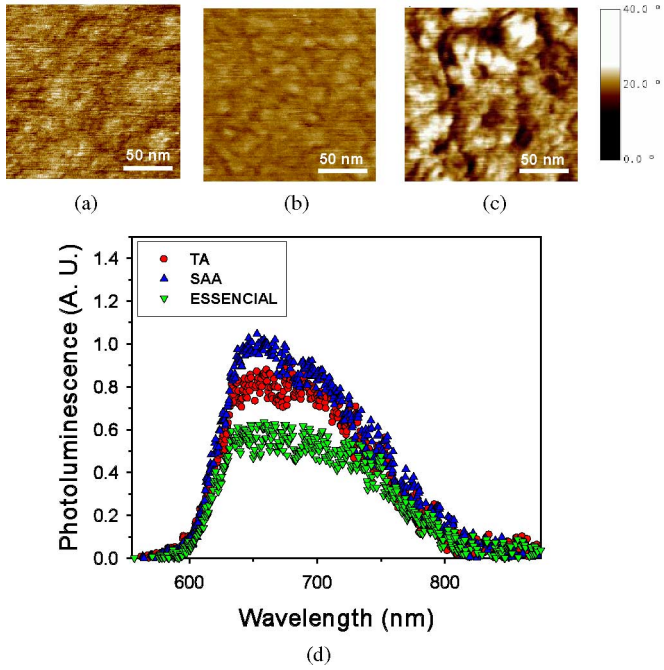

Fig. 18. (a)–(c) AFM phase images. (d) PL spectra. The images in (a)–(c) and the curves in (d) correspond to thermal-annealed sample, solvent-assisted annealed sample, and 1-min heat-treated ESSENCIAL sample, respectively. Copyright Wiley-VCH Verlag GmbH & Co. KGaA. Reproduced with permission from [50].

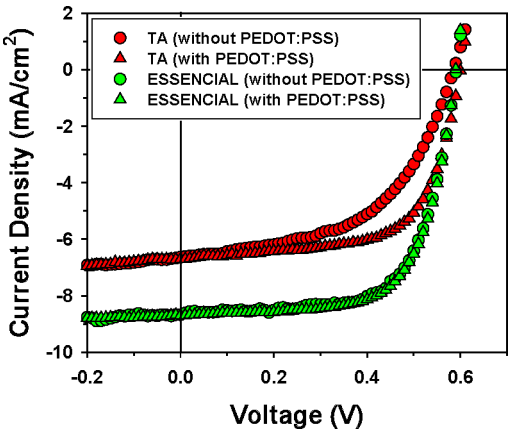

Fig. 19. *J–V* curves of thermal-annealed devices and 1-min heat-treated ESSENCIAL devices.

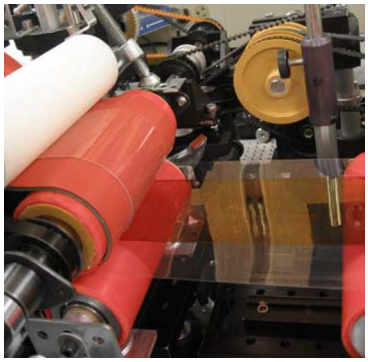

Fig. 20. Photograph of the R2R apparatus and the resultant flexible polymer solar cell before electrode deposition. Copyright Wiley-VCH Verlag GmbH & Co. KGaA. Reproduced with permission from [50].

TABLE IV
PERFORMANCES OF DEVICES FABRICATED BY DIFFERENT PROCESSING METHODS

Method	V_{oc} (V)	J_{sc} (mAcm^{-2})	FF	PCE	R_s (Ωcm^2)
Spin-casting	0.64	5.01	0.62	2.05	14.5
TA	0.60	6.46	0.65	2.53	3.3
SAA	0.57	7.75	0.67	2.96	2.0
[a]ESSENCIAL	0.59	8.75	0.69	3.50	1.2
[b]Roll-to-roll	0.59	8.71	0.67	3.45	1.4

[a]ESSENCIAL sample was further treated by heat for 1 min
[b]The solar cells fabricated by R2R processing were prepared without PEDOT:PSS layer.

the processing time as it eliminates the PEDOT:PSS coating and the baking step to remove residual H_2O molecules from PEDOT:PSS used in conventional fabrications, which is especially attractive for high-speed R2R processing.

The advantages of ESSENCIAL method to induce superior BHJ morphology in short processing time pave the way to scalable high-efficiency polymer solar cell fabrication. Here, we demonstrated fabrication of polymer solar cells using an R2R apparatus composed of dual rollers and tensioned belt covered with gas-permeable silicone film, which enables coating of the P3HT:PCBM polymer blend with uniform thickness and fast solvent evaporation in a continuous fashion (see Fig. 20). According to the dynamic elastic contact model developed for the R2R nanoimprinting [59], the thickness of coated active layer can be controlled by the solution concentration and roller pressure, which is the same condition as the small-scale ESSENCIAL experiment discussed earlier, and the film uniformity can be preserved by the belt tension during the solvent evaporation process. Fig. 20 show 3-in-wide uniform BHJ active layer film made of P3HT:PCBM blend on an ITO-coated PET substrate using the continuous R2R process. After 1-min baking, the deposition of LiF and Al cathode complete final devices.

C. Device Performances of OSCs

The device performances including PCE and *J–V* curves were measured under AM 1.5G simulated sun light (at 100 mW·cm^{-2} intensity). In device fabrication, isolated island-type metallic cathode was used to exclude the overestimation of the photocurrent commonly occurred in devices using crossbar-type electrodes [60], [90]. The patterned crossbar-type electrode geometry is the most commonly used configuration for OLEDs because this structure allows easy addressing of individual pixels. The same crossbar-type electrode geometry has been adapted to OSC fabrication for the same convenience by many laboratories. However, we found that while acceptable for OLEDs, the crossbar-type electrode geometry can lead to an incorrect analysis of PCE of the OSCs. We observed that the solar cells having the island-type electrode geometry gave a consistent cell performance, but the performance of the crossbar-type cells varied greatly depending on the size of the illuminated light beam on the cells relative to the overlapped area of the crossbar electrodes [87]. When the illuminated area was larger than the overlapped area of the crossbar electrodes, even though there was no ITO electrode outside the overlapped region, the conductive PEDOT:PSS layer plays the role of an effective anode. In other words, the crossbar-type cells can be regarded as composed of two OSCs connected in parallel: one is the solar cell having ITO anode and cathode in the overlapped region, and other is a parasitic one having PEDOT:PSS as an effective anode instead of ITO. To prove this, we built PEDOT:PSS/P3HT:PCBM/LiF/Al OSCs on a glass substrate without ITO to mimic the parasitic OSCs. Indeed, the devices showed photovoltaic characteristic, but with an FF of only 0.25, which is much smaller than the FF of 0.61 of the equivalent device having ITO [87]. This also explains why the decrease of FF of the crossbar-type OSCs is accompanied by the increase of J_{sc} when the illuminated beam size increased, which is due to the contribution of the parasitic OSC to the total measured J_{sc}. Our experiments showed that PCE could be overestimated as much as by 30%, and this could be even higher depending on electrode design and measurement conditions [90].

Using the isolated island-type Al cathode, the performances of the devices depending on the processing methods were summarized in Table IV. The values reported in the table are averaged using the data obtained by at least 20 cells. The devices fabricated by the ESSENCIAL method followed by the thermal treatment showed the highest PCE due to the optimized domain morphologies and charge pathways that resulted in both increased short-circuit current and FF. The favorable morphology also led to the lowest series resistance ($R_s \sim 1.2\ \Omega\cdot\text{cm}^2$), as expected. The devices fabricated by the R2R process, the scalable version of the ESSENCIAL process, also show the comparable PCE ($\sim$3.5%). We believe that this new process is equally applicable to BHJ structures using other materials (e.g., the low-bandgap polymer semiconductors that demonstrated higher PCE [91]), making it a potential manufacturing technique for mass production of low-cost and high-efficiency polymer solar cells.

V. CONCLUSION

We reviewed the recent progress in the area of TMEs, OSC efficiency enhancement by SPR in periodic Ag nanowire electrode, and by new processing method of organic materials. Transparent electrodes based on metallic nanostructure have proved to be a strong candidate as a replacement of conventional

ITO electrode. They have high optical transparency and good electrical conductivity. Moreover, unlike ITO, these properties can be adjusted relatively independently by changing the metal linewidth and thickness in the metal grid structure. Furthermore, they exhibit a greater flexibility than conventional ITO. Not only do metal electrodes provide excellent characteristics mentioned earlier, but also nanoscale metallic nanowire structures exhibit unique optical properties due to the excitation of SPs, which has been exploited in specially designed solar cells to achieve enhanced light absorption, and thus, enhanced PCE. About 35% enhancement of PCE was demonstrated for the OSC using transparent Ag nanowire electrode as compared with the device using conventional ITO electrode. Further enhancement is possible by designing optimal structure of Ag nanowires to match the peak absorption in the organic materials. In addition, the novel ESSENCIAL-based technique shows the most optimum BHJ morphology compared with conventional methods and permits us to realize high-efficiency polymer solar cell using high-speed R2R process. We believe that the works highlighted in this paper may help to realize low-cost, high-efficiency, and large-area OSCs.

ACKNOWLEDGMENT

The authors would like to thank Dr. X. Luo for useful discussions on the plasmonic-enhanced OSCs.

REFERENCES

[1] P. Peumans, A. Yakimov, and S. R. Forrest, "Small molecular weight organic thin-film photodetectors and solar cells," *J. Appl. Phys.*, vol. 93, pp. 3693–3723, 2003.

[2] H. Hoppe and N. S. Sariciftci, "Organic solar cells: An overview," *J. Mater. Res.*, vol. 19, pp. 1924–1945, 2004.

[3] K. M. Coakley and M. D. McGehee, "Conjugated polymer photovoltaic cells," *Chem. Mater.*, vol. 16, pp. 4533–4542, 2004.

[4] C. W. Tang, "Two-layer organic photovoltaic cell," *Appl. Phys. Lett.*, vol. 48, pp. 183–185, 1986.

[5] G. Li, V. Shrotriya, J. Huang, Y. Yao, T. Moriarty, K. Emery, and Y. Yang, "High-efficiency solution processable polymer photovoltaic cells by self-organization of polymer blends," *Nature Mater.*, vol. 4, pp. 864–868, 2005.

[6] W. Ma, C. Yang, X. Gong, K. Lee, and A. J. Heeger, "Thermally stable, efficient polymer solar cells with nanoscale control of the interpenetrating network morphology," *Adv. Funct. Mater.*, vol. 15, pp. 1617–1622, 2005.

[7] J. Y. Kim, K. Lee, N. E. Coates, D. Moses, T.-Q. Nguyen, M. Dante, and A. J. Heeger, "Efficient tandem polymer solar cells fabricated by all-solution processing," *Science*, vol. 317, pp. 222–225, 2007.

[8] S. H. Park, A. Roy, S. Beaupre, S. Cho, N. Coates, J. S. Moon, D. Moses, M. Leclerc, K. Lee, and A. J. Heeger, "Bulk heterojunction solar cells with internal quantum efficiency approaching 100%," *Nature Photon.*, vol. 3, pp. 297–302, 2009.

[9] W.-Y. Wong, X.-Z. Wang, Z. He, A. B. Djurisic, C.-T. Yip, K.-Y. Cheung, H. Wang, C. S. K. Mak, and W.-K. Chan, "Metallated conjugated polymers as a new avenue towards high-efficiency polymer solar cells," *Nature Mater.*, vol. 6, pp. 521–527, 2007.

[10] W.-Y. Wong, "Metallopolyyne polymers as new functional materials for photovoltaic and solar cell applications," *Macromol. Chem. Phys.*, vol. 209, pp. 14–24, 2008.

[11] D. Gilles, C. S. Markus, and J. B. Christoph, "Polymer-fullerene bulk-heterojunction solar cells," *Adv. Mater.*, vol. 21, pp. 1323–1338, 2009.

[12] A. Andersson, N. Johansson, P. Bröms, N. Yu, D. Lupo, and W. R. Salaneck, "Fluorine tin oxide as an alternative to indium tin oxide in polymer LEDs," *Adv. Mater.*, vol. 10, pp. 859–863, 1998.

[13] V. Adamovich, A. Shoustikov, and M. E. Thompson, "TiN as an anode material for organic light-emitting diodes," *Adv. Mater.*, vol. 11, pp. 727–730, 1999.

[14] H. Kim, C. M. Gilmore, J. S. Horwitz, A. Pique, H. Murata, G. P. Kushto, R. Schlaf, Z. H. Kafafi, and D. B. Chrisey, "Transparent conducting aluminum-doped zinc oxide thin films for organic light-emitting devices," *Appl. Phys. Lett.*, vol. 76, pp. 259–261, 2000.

[15] J. Cui, A. Wang, N. L. Edleman, J. Ni, P. Lee, N. R. Armstrong, and T. J. Marks, "Indium tin oxide alternatives-high work function transparent conducting oxides as anodes for organic light-emitting diodes," *Adv. Mater.*, vol. 13, pp. 1476–1480, 2001.

[16] F. Zhang, M. Johansson, M. R. Andersson, J. C. Hummelen, and O. Inganäs, "Polymer photovoltaic cells with conducting polymer anodes," *Adv. Mater.*, vol. 14, pp. 662–665, 2002.

[17] Z. Wu, Z. Chen, X. Du, J. M. Logan, J. Sippel, M. Nikolou, K. Kamaras, J. R. Reynolds, D. B. Tanner, A. F. Hebard, and A. G. Rinzler, "Transparent, conductive carbon nanotube films," *Science*, vol. 305, pp. 1273–1276, 2004.

[18] A. J. Miller, R. A. Hatton, and S. R. P. Silva, "Interpenetrating multiwall carbon nanotube electrodes for organic solar cells," *Appl. Phys. Lett.*, vol. 89, pp. 133117-1–133117-3, 2006.

[19] J. van de Lagemaat, T. M. Barnes, G. Rumbles, S. E. Shaheen, T. J. Coutts, C. Weeks, I. Levitsky, J. Peltola, and P. Glatkowski, "Organic solar cells with carbon nanotubes replacing In_2 O_3:Sn as the transparent electrode," *Appl. Phys. Lett.*, vol. 88, pp. 233503-1–233503-3, 2006.

[20] M. W. Rowell, M. A. Topinka, M. D. McGehee, H.-J. Prall, G. Dennler, N. S. Sariciftci, L. Hu, and G. Gruner, "Organic solar cells with carbon nanotube network electrodes," *Appl. Phys. Lett.*, vol. 88, pp. 233506-1–233506-3, 2006.

[21] F. Yang and S. R. Forrest, "Organic solar cells using transparent SnO_2-F anodes," *Adv. Mater.*, vol. 18, pp. 2018–2022, 2006.

[22] A. J. Anthony, R. A. Hatton, G. Y. Chen, and S. R. P. Silva, "Carbon nanotubes grown on In_2 O_3:Sn glass as large area electrodes for organic photovoltaics," *Appl. Phys. Lett.*, vol. 90, pp. 023105-1–023105-3, 2007.

[23] K. Tvingstedt and O. Inganäs, "Electrode grids for ITO free organic photovoltaic devices," *Adv. Mater.*, vol. 19, pp. 2893–2897, 2007.

[24] J.-Y. Lee, S. T. Connor, Y. Cui, and P. Peumans, "Solution-processed metal nanowire mesh transparent electrodes," *Nano Lett.*, vol. 8, pp. 689–692, 2008.

[25] M.-G. Kang, M.-S. Kim, J. Kim, and L. J. Guo, "Organic solar cells using nanoimprinted transparent metal electrodes," *Adv. Mater.*, vol. 20, pp. 4408–4413, 2008.

[26] S. K. Park, J. I. Han, W. K. Kim, and M. G. Kwak, "Deposition of indium-tin-oxide films on polymer substrates for application in plastic-based flat panel displays," *Thin Solid Films*, vol. 397, pp. 49–55, 2001.

[27] F. L. Wong, M. K. Fung, S. W. Tong, C. S. Lee, and S. T. Lee, "Flexible organic light-emitting device based on magnetron sputtered indium-tin-oxide on plastic substrate," *Thin Solid Films*, vol. 466, pp. 225–230, 2004.

[28] J. Szczyrbowski, A. Dietrich, and H. Hoffmann, "Optical and electrical properties of RF-sputtered indium-tin oxide films," *Phys. Stat. Sol. A*, vol. 78, pp. 243–252, 1983.

[29] K. Sreenivas, T. S. Rao, A. Mansingh, and S. Chandra, "Preparation and characterization of rf sputtered indium tin oxide films," *J. Appl. Phys.*, vol. 57, pp. 384–392, 1985.

[30] M. Higuchi, S. Uekusa, R. Nakano, and K. Yokogawa, "Postdeposition annealing influence on sputtered indium tin oxide film characteristics," *Jpn. J. Appl. Phys.*, vol. 1, pp. 302–306, 1994.

[31] S. Yamamoto, T. Yamanaka, and Z. Ueda, "Properties of Sn-doped In_2 O_3 by reactive magnetron sputtering and subsequent annealing," *J. Vac. Sci. Technol. A*, vol. 5, pp. 1952–1955, 1987.

[32] T. Minami, H. Sonohara, T. Kakumu, and S. Takata, "Physics of very thin ITO conducting films with high transparency prepared by DC magnetron sputtering," *Thin Solid Films*, vol. 270, pp. 37–42, 1995.

[33] F. Niino, H. Hirasawa, and K.-I. Kondo, "Deposition of low-resistivity ITO on plastic substrates by DC arc-discharge ion plating," *Thin Solid Films*, vol. 411, pp. 28–31, 2002.

[34] J. R. Sheats and D. B. Roitman, "Failure modes in polymer-based light-emitting diodes," *Synth. Met.*, vol. 95, pp. 79–85, 1998.

[35] Z. Chen, B. Cotterell, W. Wang, E. Guenther, and S.-J. Chua, "A mechanical assessment of flexible optoelectronic devices," *Thin Solid Films*, vol. 394, pp. 202–206, 2001.

[36] W. S. Jahng, A. H. Francis, H. Moon, J. I. Nanos, and M. D. Curtis, "Is indium tin oxide a suitable electrode in organic solar cells? Photovoltaic properties of interfaces in organic p/n junction photodiodes," *Appl. Phys. Lett.*, vol. 88, pp. 093504-1–093504-3, 2006.

[37] B. Maennig, J. Drechsel, D. Gebeyehu, P. Simon, F. Kozlowski, A. Werner, F. Li, S. Grundmann, S. Sonntag, M. Koch, K. Leo, M. Pfeiffer, H. Hoppe, D. Meissner, N. S. Sariciftci, I. Riedel, V. Dyakonov, and J. Parisi, "Organic p-i-n solar cells," *Appl. Phys. A*, vol. 79, pp. 1–14, 2004.

[38] Y.-H. Kim, S.-H. Lee, J. Noh, and S.-H. Han, "Performance and stability of electroluminescent device with self-assembled layers of poly(3,4-ethylenedioxythiophene)-poly(styrenesulfonate) and polyelectrolytes," *Thin Solid Films*, vol. 510, pp. 305–310, 2006.

[39] M. P. De Jong, D. P. L. Simons, M. A. Reijme, L. J. van Ijzendoorn, A. W. Denier Van DerGon, M. J. A. de Voigt, H. H. Brongersma, and R. W. Gymer, "Indium diffusion in model polymer light-emitting diodes," *Synth. Met.*, vol. 110, pp. 1–6, 2000.

[40] G. Yu, J. Gao, J. C. Hummelen, F. Wudl, and A. J. Heeger, "Polymer photovoltaic cells: Enhanced efficiencies via a network of internal donor-acceptor heterojunctions," *Science*, vol. 270, pp. 1789–1791, 1995.

[41] J. J. M. Halls, C. A. Walsh, N. C. Greenham, E. A. Marseglia, R. H. Friend, S. C. Moratti, and A. B. Holmes, "Efficient photodiodes from interpenetrating polymer networks," *Nature*, vol. 376, pp. 498–500, 1995.

[42] S. S. V. Bavel, E. Sourty, G. D. With, and J. Loos, "Three-dimensional nanoscale organization of bulk heterojunction polymer solar cells," *Nano Lett.*, vol. 9, pp. 507–513, 2009.

[43] J. M. Halls, K. Pichler, R. H. Friend, S. C. Moratti, and A. B. Holmes, "Exciton diffusion and dissociation in a poly(p-phenylenevinylene)/C_{60} heterojunction photovoltaic cell," *Appl. Phys. Lett.*, vol. 68, pp. 3120–3122, 1996.

[44] L. A. A. Pettersson, L. S. Roman, and O. Inganäs, "Modeling photocurrent action spectra of photovoltaic devices based on organic thin films," *J. Appl. Phys.*, vol. 86, pp. 487–496, 1999.

[45] M. Theander, A. Yartsev, D. Zigmantas, V. Sundström, W. Mammo, M. R. Anderson, and O. Inganäs, "Photoluminescence quenching at a polythiophene/C_{60} heterojunction," *Phys. Rev. B*, vol. 61, pp. 12957–12963, 2000.

[46] T. J. Savenije, J. M. Warman, and A. Goossens, "Visible light sensitisation of titanium dioxide using a phenylene vinylene polymer," *Chem. Phys. Lett.*, vol. 287, pp. 148–153, 1998.

[47] A. Haugeneder, M. Neges, C. Kallinger, W. Spirkl, U. Lemmer, J. Feldman, U. Scherf, E. Harth, A. Gugel, and K. Mullen, "Exciton diffusion and dissociation in conjugated polymer/fullerene blends and heterostructures," *Phys. Rev. B*, vol. 59, pp. 15346–15351, 1999.

[48] M.-G. Kang and L. J. Guo, "Nanoimprinted semitransparent metal electrodes and their application in organic light emitting diodes," *Adv. Mater.*, vol. 19, pp. 1391–1396, 2007.

[49] L. J. Guo, "Nanoimprint lithography: Methods and material requirements," *Adv. Mater.*, vol. 19, pp. 495–513, 2007.

[50] H. J. Park, M.-G. Kang, S. H. Ahn, and L. J. Guo, "Facile route to polymer solar cells with optimum morphology readily applicable to roll-to-roll process without sacrificing high device performances," *Adv. Mater.*, to be published. DOI: 10.1002/adma.201000250

[51] L. S. Roman, O. Inganäs, T. Granlund, T. Nyberg, M. Svensson, M. R. Andersson, and J. C. Hummelen, "Trapping light in polymer photodiodes with soft embossed gratings," *Adv. Mater.*, vol. 12, pp. 189–195, 2000.

[52] S.-S. Kim, S.-I. Na, J. Jo, and D.-Y. Kim, "Efficient polymer solar cells fabricated by simple brush painting," *Adv. Mater.*, vol. 19, pp. 4410–4415, 2007.

[53] C. Cocoyer, L. Rocha, L. Sicot, B. Geffroy, R. D. Bettignies, C. Sentein, C. Fiorini-Debuisschert, and P. Raimond, "Implementation of submicrometric periodic surface structures toward improvement of organic-solar-cell performances," *Appl. Phys. Lett.*, vol. 88, pp. 133108-1–133108-3, 2006.

[54] M.-S. Kim, J.-S. Kim, J. C. Cho, M. Shtein, L. J. Guo, and J. Kim, "Flexible conjugated polymer photovoltaic cells with controlled heterojunctions fabricated using nanoimprint lithography," *Appl. Phys. Lett.*, vol. 90, pp. 123113-1–123113-3, 2007.

[55] S. H. Ahn and L. J. Guo, "High-speed roll-to-roll nanoimprint lithography on flexible plastic substrates," *Adv. Mater.*, vol. 20, pp. 2044–2049, 2008.

[56] S. Y. Chou, P. R. Krauss, and P. J. Renstrom, "Imprint lithography with 25-nanometer resolution," *Science*, vol. 272, pp. 85–87, 1996.

[57] M.-G. Kang and L. J. Guo, "Semitransparent Cu electrode on a flexible substrate and its application in organic light emitting diodes," *J. Vac. Sci. Technol. B*, vol. 25, pp. 2637–2641, 2007.

[58] M.-G. Kang, H. J. Park, S. H. Ahn, and L. J. Guo, "Transparent Cu nanowire mesh electrode on flexible substrates fabricated by transfer printing and its application in organic solar cells," *Sol. Energy Mater. Sol. Cells*, vol. 94, pp. 1179–1184, 2010.

[59] S. H. Ahn and L. J. Guo, "Large-area roll-to-roll and roll-to-plate nanoimprint lithography and analytical models for predicting residual layer thickness," *ACS Nano*, vol. 3, pp. 2304–2310, 2009.

[60] A. Cravino, P. Schilinsky, and C. J. Brabec, "Characterization of organic solar cells: The importance of device layout," *Adv. Funct. Mater.*, vol. 17, pp. 3906–3910, 2007.

[61] G. Li, V. Shrotriya, Y. Yao, J. Huang, and Y. Yang, "Manipulating regioregular poly(3-hexylthiophene): [6,6]-phenyl-C61-butyric acid methyl ester blends—Route towards high efficiency polymer solar cells," *J. Mater. Chem.*, vol. 17, pp. 3126–3140, 2007.

[62] P. W. M. Blom, V. D. Mihailetchi, L. J. A. Koster, and D. E. Markov, "Device physics of polymer:fullerene bulk heterojunction solar cells," *Adv. Mater.*, vol. 19, pp. 1551–1566, 2007.

[63] S.-B. Rim, S. Zhao, S. R. Scully, M. D. McGehee, and P. Peumans, "An effective light trapping configuration for thin-film solar cells," *Appl. Phys. Lett.*, vol. 91, pp. 243501-1–243501-3, 2007.

[64] S.-I. Na, S.-S. Kim, S.-S. Kwon, J. Jo, J. Kim, T. Lee, and D.-Y. Kim, "Surface relief gratings on poly(3-hexylthiophene) and fullerene blends for efficient organic solar cells," *Appl. Phys. Lett.*, vol. 91, pp. 173509-1–173509-3, 2007.

[65] D.-H. Ko, J. R. Tumbleston, L. Zhang, S. Williams, J. M. DeSimone, R. Lopez, and E. T. Samulski, "Photonic crystal geometry for organic solar cells," *Nano Lett.*, vol. 9, pp. 2742–2746, 2009.

[66] C. Stephane, P. Fabrice, T. Roland, and P. Jean-Luc, "Efficient light absorption in metal-semiconductor-metal nanostructures," *Appl. Phys. Lett.*, vol. 85, pp. 194–196, 2004.

[67] P. R. Barry, P. Peter, and R. F. Stephen, "Long-range absorption enhancement in organic tandem thin-film solar cells containing silver nanoclusters," *J. Appl. Phys.*, vol. 96, pp. 7519–7526, 2004.

[68] T. D. Heidel, J. K. Mapel, M. Singh, K. Celebi, and M. A. Baldo, "Surface plasmon polariton mediated energy transfer in organic photovoltaic devices," *Appl. Phys. Lett.*, vol. 91, pp. 093506-1–093506-3, 2007.

[69] J. K. Mapel, M. Singh, M. A. Baldo, and K. Celebi, "Plasmonic excitation of organic double heterostructure solar cells," *Appl. Phys. Lett.*, vol. 90, pp. 121102-1–121101-3, 2007.

[70] A. J. Morfa, K. L. Rowlen, T. H. R. ReillyIII, M. J. Romero, and J. V. D. Lagemaat, "Plasmon-enhanced solar energy conversion in organic bulk heterojunction photovoltaics," *Appl. Phys. Lett.*, vol. 92, pp. 013504-1–013504-3, 2008.

[71] S.-S. Kim, S.-I. Na, J. Jo, D.-Y. Kim, and Y.-C. Nah, "Plasmon enhanced performance of organic solar cells using electrodeposited Ag nanoparticles," *Appl. Phys. Lett.*, vol. 93, pp. 073307-1–073307-3, 2008.

[72] T. H. Reilly, III, J. van de Lagemaat, R. C. Tenent, A. J. Morfa, and K. L. Rowlen, "Surface-plasmon enhanced transparent electrodes in organic photovoltaics," *Appl. Phys. Lett.*, vol. 92, pp. 243304-1–243304-3, 2008.

[73] N. C. Lindquist, W. A. Luhman, S.-H. Oh, and R. J. Homes, "Plasmonic nanocavity arrays for enhanced efficiency in organic photovoltaic cells," *Appl. Phys. Lett.*, vol. 93, pp. 123308-1–123308-3, 2008.

[74] M. G. Kang, T. Xu, H. J. Park, X. G. Luo, and L. J. Guo, "Efficiency enhancement of organic solar cells using transparent plasmonic Ag nanowire electrodes," *Adv. Mater.*, vol. 22, no. 39, pp. 4378–4383, Oct. 2010.

[75] M. D. Malinsky, K. L. Kelly, G. C. Schatz, and R. P. Van Duyne, "Nanosphere Lithography: Effect of substrate on the localized surface plasmon resonance spectrum of silver nanoparticles," *J. Phys. Chem. B*, vol. 105, pp. 2343–2350, 2001.

[76] M. Campoy-Quiles, T. Ferenczi, T. Agostinelli, P. G. Etchegoin, Y. Kim, T. D. Anthopoulos, P. N. Stavrinou, D. D. C. Bradley, and J. Nelson, "Morphology evolution via self-organization and lateral and vertical diffusion in polymer:fullerene solar cell blends," *Nature Mater.*, vol. 7, pp. 158–164, 2008.

[77] Y. Yao, J. Hou, Z. Xu, G. Li, and Y. Yang, "Effects of solvent mixtures on the nanoscale phase separation in polymer solar cells," *Adv. Funct. Mater.*, vol. 18, pp. 1783–1789, 2008.

[78] Z. Xu, L.-M. Chen, G. Yang, C.-H. Huang, J. Hou, Y. Wu, G. Li, C.-S. Hsu, and Y. Yang, "Vertical phase separation in poly(3-hexylthiophene):fullerene derivative blends and its advantage for inverted structure solar cells," *Adv. Funct. Mater.*, vol. 19, pp. 1227–1234, 2009.

[79] D. S. Germack, C. K. Chan, B. H. Hamadani, L. J. Richter, D. A. Fischer, D. J. Gundlach, and D. M. DeLongchamp, "Substrate-dependent interface composition and charge transport in films for organic photovoltaics," *Appl. Phys. Lett.*, vol. 94, pp. 233303-1–233303-3, 2009.

[80] F. C. Krebs, S. A. Gevorgyan, and J. Alstrup, "A roll-to-roll process to flexible polymer solar cells: Model studies, manufacture and operational stability studies," *J. Mater. Chem.*, vol. 19, pp. 5442–5451, 2009.

[81] F. C. Krebs, "All solution roll-to-roll processed polymer solar cells free from indium-tin-oxide and vacuum coating steps," *Org. Electron.*, vol. 10, pp. 761–768, 2009.
[82] L. Blankenburg, K. Schultheis, H. Schache, S. Sensfuss, and M. Schrödner, "Reel-to-reel wet coating as an efficient up-scaling technique for the production of bulk-heterojunction polymer solar cells," *Sol. Energy Mater. Sol. Cells*, vol. 93, pp. 476–483, 2009.
[83] M. Sunderberg, O. Inganas, S. Stafstrom, G. Gustafsson, and B. Sjogren, "Optical absorption of poly(3-alkylthiophenes) at low temperatures," *Solid State Commun.*, vol. 71, pp. 435–439, 1989.
[84] V. D. Mihailetchi, L. J. A. Koster, P. W. M. Blom, C. Melzer, B. D. Boer, J. K. J. Duren, and R. A. J. Janssen, "Compositional dependence of the performance of poly(p-phenylene vinylene):methanofullerene bulk-heterojunction solar cells," *Adv. Funct. Mater.*, vol. 15, pp. 795–801, 2005.
[85] V. Shrotriya, Y. Yao, G. Li, and Y. Yang, "Effect of self-organization in polymer/fullerene bulk heterojunctions on solar cell performance," *Appl. Phys. Lett.*, vol. 89, pp. 063505-1–063505-3, 2006.
[86] M. A. Lampert and P. Mark, *Current Injection in Solids*. New York: Academic, 1970.
[87] Y. Kim, S. Cook, S. M. Tuladhar, S. A. Choulis, J. Nelson, J. R. Durrant, D. D. C. Bradley, M. Giles, I. Mcculloch, C.-S. Ha, and M. Ree, "A strong regioregularity effect in self-organizing conjugated polymer films and high-efficiency polythiophene:fullerene solar cells," *Nature Mater.*, vol. 5, pp. 197–203, 2006.
[88] N. Koch, A. Elschner, and R. L. Johnson, "Green polyfluorene-conducting polymer interfaces: Energy level alignment and device performance," *J. Appl. Phys.*, vol. 100, pp. 024512-1–024512-5, 2006.
[89] M. D. Irwin, D. B. Buchholz, A. W. Hains, R. P. H. Chang, and T. J. Marks, "p-Type semiconducting nickel oxide as an efficiency-enhancing anode interfacial layer in polymer bulk-heterojunction solar cells," *Proc. Natl. Acad. Sci. USA*, vol. 105, pp. 2783–2787, 2008.
[90] M.-S. Kim, M.-G. Kang, L. J. Guo, and J. Kim, "Choice of electrode geometry for accurate measurement of organic photovoltaic cell performance," *Appl. Phys. Lett.*, vol. 92, pp. 133301-1–133301-3, 2008.
[91] H.-Y. Chen, J. Hou, S. Zhang, Y. Liang, G. Yang, Y. Yang, L. Yu, Y. Wu, and G. Li, "Polymer solar cells with enhanced open-circuit voltage and efficiency," *Nature Photon.*, vol. 3, pp. 649–653, 2009.

Myung-Gyu Kang received the B.S. degree in electrical engineering from Kyungpook National University, Daegu, Korea, in 2000, the M.S. degree in electrical engineering from the Korea Advanced Institute Science and Technology, Daejeon, Korea, in 2002, and the Ph.D. degree in electrical engineering from the University of Michigan, Ann Arbor, in 2009.

From 2009 to until early 2010, he was a Postdoctoral Researcher at the University of Michigan. He is currently with the National Institute of Standards and Technology, Gaithersburg, MD. His research interests include nanofabrication technology, plasmonic nanostructures, and organic and inorganic optoelectronic devices.

Hui Joon Park received the B.S. and M.S. degrees in materials science and engineering from Seoul National University, Seoul, Korea, in 2002 and 2004, respectively. He is currently working toward the Ph.D. degree in organic electronics and photonics at the University of Michigan, Ann Arbor.

From 2004 to 2006, he was with LG Electronics. From 2006 to 2007, he was a Research Scientist at the Korea Institute of Science and Technology, Seoul. He has been a member of the Solid State Electronics Laboratory, Department of Electrical Engineering and Computer Science, University of Michigan.

Se Hyun Ahn received the B.S. degree in mechanical engineering from Yonsei University, Seoul, Korea, in 2001, and the M.S. degree in mechanical engineering from Seoul National University, Seoul, in 2003. He is currently working toward the Ph.D. degree in mechanical engineering at the University of Michigan, Ann Arbor.

From 2003 to 2004, he was with LG Electronics, Korea. He has been a Graduate Student Research Assistant in the Solid State Electronics Laboratory, University of Michigan, where he has been engaged in the development of high-speed, high-throughput, nanopatterning processes including roll-to-roll nanoimprint lithography and Dynamic Nano-Inscribing for displays and energy applications.

Ting Xu received the dual B.S. degrees in optical information technology and computer science from the Nanjing University of Posts and Telecommunications, Nanjing, China, in 2006. He is currently working toward the joint Ph.D. degree from the Chinese Academy of Sciences, Chengdu, China, and University of Michigan, Ann Arbor.

His current research interests include plasmonic nanodevices, nanofabrication technology, and metamaterials.

L. Jay Guo received the M.S. and Ph.D. degrees in electrical engineering from the University of Minnesota, Minneapolis, in 1995 and 1997, respectively.

From 1998 to 1999, he was a Research Associate at Princeton University, Princeton, NJ. Since 1999, he has been in the Department of Electrical Engineering and Computer Science, University of Michigan, Ann Arbor, where he is currently an Associate Professor. His research interests include polymer-based photonic devices and sensor applications, plasmonic nanophtonics, organic electronics and photonics, and nanoimprint technology and applications.